Journal of Oceanography, Vol. 63, pp. 379 to 391, 2007

Anticyclonic Eddy Caused by the Soya Warm Current in an Okhotsk OGCM

Keisuke Uchimoto[1]*, Humio Mitsudera[1], Naoto Ebuchi[2] and Yasumasa Miyazawa[3]

[1]*Pan-Okhotsk Research Center, Institute of Low Temperature Science, Hokkaido University, Kita-ku, Sapporo, Hokkaido 060-0819, Japan*
[2]*Institute of Low Temperature Science, Hokkaido University, Kita-ku, Sapporo, Hokkaido 060-0819, Japan*
[3]*Frontier Research System for Global Change/JAMSTEC, Showamachi, Kanazawa-ku, Yokohama, Kanagawa 236-0001, Japan*

(Received 10 January 2006; in revised form 11 December 2006; accepted 25 December 2006)

An OGCM of the Sea of Okhotsk with a 1/12° horizontal resolution and 45 vertical levels has been constructed, which successfully represents characteristics of its circulations. This article focuses particularly on an anticyclonic eddy forming off Hokkaido in the OGCM. It forms in late summer when the warm and saline Soya Warm Current Water separates from the northeastern coast of Hokkaido. This eddy is identified as the eddy studied by Wakatsuchi and Martin (1991) since its location, evolution and vertical structure are consistent with their description. Numerical experiments with varying transport of the Soya Warm Current (SWC) have been carried out, where the transport of the SWC is changed by applying the Island Rule around Hokkaido. It is shown that the eddy formation depends on the transport of the SWC. When the transport is large, an eddy forms off the Shiretoko Peninsula. When the transport is small, however, the saline Soya Warm Current Water does not reach that area, nor does a distinct eddy form. It is when the inflow transport of the Soya Warm Current is larger than the outflow from the Nemuro Strait and the Kunashiri Channel that the anticyclonic eddy forms.

Keywords:
· Anticyclonic eddy,
· Kuril Basin,
· Soya Warm Current,
· Sea of Okhotsk,
· OGCM,
· numerical experiment,
· Island Rule.

1. Introduction

The Sea of Okhotsk may be divided roughly into two parts from the viewpoint of the gyre circulation; one is the central and northern basin with a cyclonic gyre, and the other is the southern basin, the Kuril Basin, with an anticyclonic gyre (Wakatsuchi and Martin, 1991, hereafter referred to as WM91; Ohshima *et al*., 2002; Simizu and Ohshima, 2006). Ohshima *et al*. (2004) showed that the cyclonic gyre in the central and northern parts of the basin is primarily driven by the positive wind stress curl over the basin. On the other hand, the anticyclonic gyre in the Kuril Basin cannot be explained by the wind stress curl in the Sea of Okhotsk. The mechanisms underlying the formation of the anticyclonic gyre in the Kuril Basin remain to be solved.

Within the anticyclonic gyre in the Kuril Basin, mesoscale eddies have been observed, and many of these eddies are also anticyclonic (WM91; Ohshima *et al*., 2002; Ebuchi, 2006). Although it is known that these anticyclonic eddies can be classified into several categories according to their vertical structure (Itoh *et al*., personal communication), there is only a small body of literature on such eddies.

Many eddies in the ocean result from hydrodynamic (baroclinic/barotropic) instability. In the Kuril Basin, eddies along the Kuril Islands that have a cold, less saline core may be generated by baroclinic instability associated with tidal mixing along the Kuril Islands (Ohshima *et al*., 2005). On the other hand, some eddies form when an inflow of low density water intrudes into a deep basin. The eddy forming off the Shiretoko Peninsula in fall is likely to be an eddy of this type. This is one of the few eddies in the Kuril Basin that have been observed in some detail. This eddy is characterized as warm, saline water near the surface, up to about 100 m deep, riding on a cold, less saline core. WM91 suggested from observations that

* Corresponding author. E-mail: uchimoto@lowtem.hokudai.ac.jp

Copyright©The Oceanographic Society of Japan/TERRAPUB/Springer

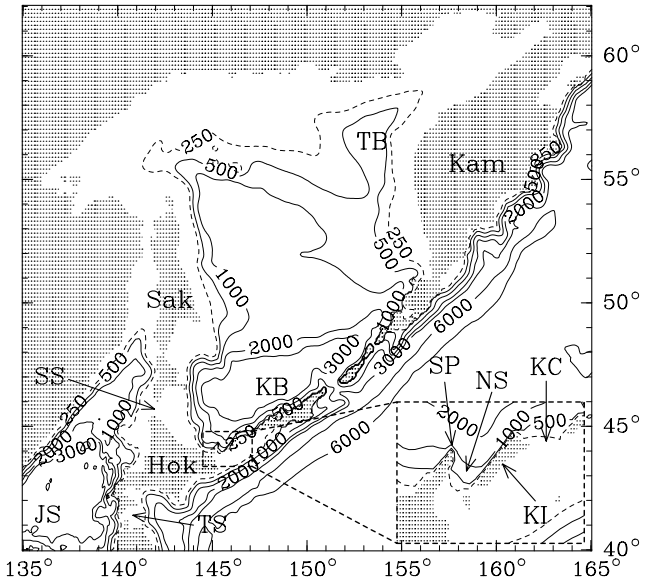

Fig. 1. Model domain and bottom topography. Abbreviations in the panel are as follows: Hok: Hokkaido, JS: Japan Sea, Kam: Kamchatka, KB: Kuril Basin, KC: Kunashiri Channel, KI: Kunashiri Island, NS: Nemuro Strait, Sak: Sakhalin, SP: Shiretoko Peninsula, SS: Soya Strait, TB: Tinro Basin, TS: Tsugaru Strait.

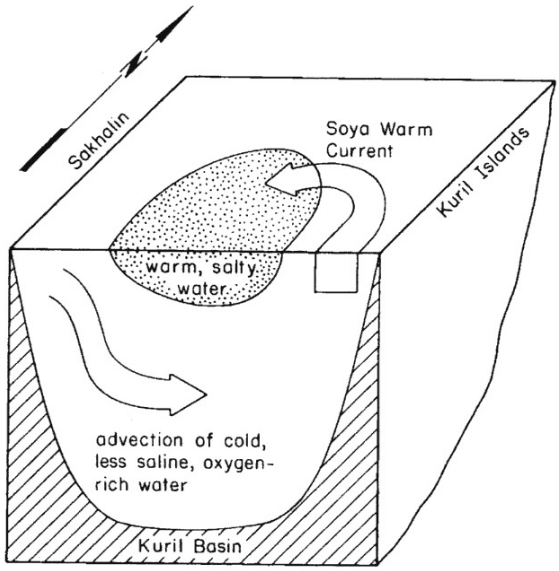

Fig. 2. Schematic picture of the WM eddy (from Wakatsuchi and Martin, 1991).

this eddy is associated with the inflow of the warm, saline Soya Warm Current Water (SWC Water) from the Shiretoko Peninsula of the northeastern coast of Hokkaido into the Kuril Basin (see Fig. 1 for geometry). Although their data was limited to two seasons (June/July and October/November) in two years (1977 and 1978), they hypothesized as in Fig. 2 (figure 14 of WM91) that in summer the lighter SWC Water spreads over the denser water that comes from the northwestern part of the Sea of Okhotsk, with the isopycnals of the upper ocean caving in so that the anticyclonic eddy forms geostrophically. The eddy observed by WM91 was located around 146°E, 46°N (see WM91's figure 3). An anticyclonic eddy with similar seasonal variations to that of WM91 is also observed by the TOPEX/POSEIDON altimeter (Ebuchi, 2006). We refer to this eddy as "the WM eddy".

Although direct observations in the Sea of Okhotsk have increased recently, areas and terms of historical data are still sparse and limited. Numerical modeling is therefore an important tool for understanding the circulation in the Sea of Okhotsk. Several numerical experiments have been conducted to simulate this circulation. For example, Simizu and Ohshima (2006) simulated wind-driven circulation in the northern basin of the Sea of Okhotsk well, including the double-core structure of the East Sakhalin Current (ESC). The evolution of sea-ice has also been investigated using a coupled ice-ocean model (Ikeda *et al*., 2004; Watanabe *et al*., 2004). However, the previous models had a relatively coarse resolution, such as 1/6°, in which eddies are marginally represented. In the present study we have constructed a high-resolution model (Okhotsk OGCM) of 1/12° resolution, which therefore resolves eddies at least in the southern basin of the Sea of Okhotsk. Further, not only is the resolution high, but the Soya Strait and some straits along the Kuril Islands are open in our model. This greatly improves the simulation of the circulation in the Kuril Basin by allowing exchanges of water among the Sea of Okhotsk, the Japan Sea and the Pacific. Owing to these characteristics of the Okhotsk OGCM, we have succeeded in reproducing various mesoscale features in the Kuril Basin, including the WM eddy, as discussed in the following sections.

In the present paper we mainly focus on the formation and evolution of the WM eddy off the northeastern coast of Hokkaido. The next section describes the Okhotsk OGCM. Section 3 outlines circulations represented in the model. The WM eddy is described in Section 4. An anticyclonic eddy reproduced in the OGCM is compared with an observed one, and is shown to be the WM eddy. Section 5 presents the numerical experiments with various transports of the Soya Warm Current. A discussion of the WM eddy formation mechanism is also given there. We show that the formation of the WM eddy is related to the transport of the Soya Warm Current. Section 6 is a summary.

2. Model

The Okhotsk OGCM is part of the model developed

for the Japan Coastal Ocean Predictability Experiment (JCOPE; see http://www.jamstec.go.jp/frcgc/jcope/), which is based on a general coordinate version of the Princeton Ocean Model (Mellor *et al*., 2002). The JCOPE model is constructed for the North Pacific, and consists of two components: a high resolution model with spatial grid of 1/12° and 45 levels is embedded in a low resolution, basin-wide model with spatial grid of 1/4° and 21 levels. The resolution of the Okhotsk OGCM is the same as that of the high resolution JCOPE model and the domain is from 135 to 165°E and from 40 to 62°N (Fig. 1). Lateral boundary conditions in the Okhotsk OGCM are determined by the results of the JCOPE model.

The model employs a z–σ coordinate, which corresponds with a σ coordinate below a certain depth z_c (which is set to $H/2$, where H is the total depth) and an almost z coordinate above. The Smagorinsky formula is used for horizontal viscosity, which gives the viscosity coefficient proportional to the horizontal grid size and velocity gradient (Smagorinsky, 1963). The proportional coefficient is chosen to be 0.06. The horizontal diffusivity is one-half of the horizontal viscosity. The vertical viscosity and diffusivity are calculated from second-moment turbulence closure (Mellor and Yamada, 1982).

The bottom topography is created from the 1/12° data, GETECH DTM5. In addition, the 500-m mesh bottom topography provided by the Hydrographic Department of Japan is embedded in the coastal sea around Japan. The bottom topography is smoothed so that the bottom slope between two adjacent grid points, $|H_1 - H_2|/|H_1 + H_2|$ (where H_1 and H_2 are depth), is not beyond 0.175. A Gaussian smoother with 1/5° scale is adopted. This modification reduces the pressure gradient error (Mellor *et al*., 1994). The topography of the Kuril Islands and straits is modified.

The JCOPE model is initiated from a state of rest with annual mean temperature and salinity (Boyer and Levitus, 1997). It is driven by wind stress, and heat and salt fluxes. The wind stress is given by QuikSCAT winds (Liu *et al*., 1998), and heat flux fields are calculated from the NCEP/NCAR reanalysis data combined with the QuikSCAT winds using the bulk formula. The wind stress and heat flux are monthly mean climatology for the first 5 years from September 1994 to August 1999, and are then switched to real-time data thereafter. Salinity at the surface is restored to the monthly mean climatology (Levitus *et al*., 1994) with a relaxing time scale of 30 days.

The Okhotsk OGCM is driven by the same surface momentum, heat and salt fluxes as those of the JCOPE model until 16 April 1999. The wind stress is then changed to that calculated from the European Center for Medium-Range Weather Forecasts reanalysis data (ERA-40) with a 1.125° × 1.125° horizontal resolution because the QuikSCAT wind may not be estimated appropriately over the sea ice. We use the formulae of Simizu and Ohshima (2002) to convert the wind velocity of ERA-40 to the stress. Note that this change from the QuikSCAT wind to the ERA-40 data does not influence the results regarding the WM eddy formation. The present study uses monthly mean climatological wind stress and heat flux. The results of the model are averaged over 10 days. Note that the Christian Era in the results is only an index showing the number of years that have passed since the initially-set year (i.e. 1994) in the model.

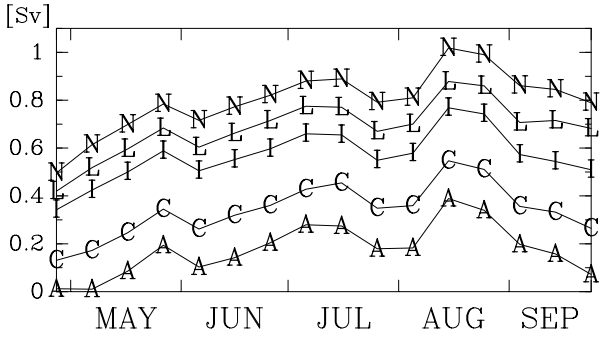

Fig. 3. Examples of time series of the transport through the Soya Strait. A, C, I, L, N denote the cases shown in Table 1.

Sea-ice dynamics and thermodynamics are not taken into account in this model. Therefore, the sea surface temperature (SST) in the model might become extremely low in winter. In order to avoid this, SST is set to be –1.8°C while heat flux is set to zero once the SST decreases below –1.8°C. The Okhotsk OGCM does not include tidal forcing. Although tidal forcing is important in modeling eddies in the Kuril Basin (e.g. Ohshima *et al*., 2005), it does not appear to greatly affect formation of the WM eddy.

In preliminary runs, the maximum transport through the Soya Strait was about 0.4 Sv, which was thought to be too small as the actual transport appears to reach about 1 Sv in summer (cf. Ebuchi *et al*., 2006). In contrast, the mean transport through the Tsugaru Strait was slightly too large. To improve it, a large constant horizontal kinematic viscosity, 5000 m^2s^{-1}, instead of the Smagorinsky parameterization, is employed in the Tsugaru Strait. The result of this run is described as Case I in Section 5, while the transport of the SWC of this case is shown in Fig. 3.

We then conducted numerical experiments to investigate the dependency of the WM eddy evolution on the transport of the SWC (Section 5). The transport of the SWC is defined as that flowing through the Soya Strait. We apply the concept of the "Island Rule" (Godfrey, 1989) to make the transport increase or decrease compared to that of Case I. As shown by Liu *et al*. (1999), a patch of

Table 1. Transport through the Soya Strait averaged over the experiment period, 160 days from 16 April to 23 September, in each case.

Case	Soya transport [Sv]
A	0.18
B	0.26
C	0.34
D	0.41
E	0.45
F	0.49
G	0.53
H	0.55
I	0.57
J	0.60
K	0.63
L	0.68
M	0.74
N	0.80
O	0.90
P	0.99
Q	1.1

wind stress around an island generates circulation around the island. Its transport is the same as that derived from the Island Rule after adjustment, i.e.,

$$T_{local} = \frac{1}{\rho(f_n - f_s)} \oint_{C_I} \boldsymbol{\tau} \cdot d\mathbf{s}, \qquad (1)$$

where $\boldsymbol{\tau}$ is the wind stress, ρ is density, f_n, f_s are the Coriolis parameters at the northern and southern tips of the island, respectively, and C_I is a counterclockwise circuit around the island. Considering the above, we impose a spatially and temporally constant eastward or westward wind stress imposed over the Tsugaru Strait to generate a constant transport, T_{local}, around Hokkaido island. The net transport around Hokkaido island, T_{Hok}, then becomes the sum of T_{local} and the original (i.e. Case I) transport, T_I,

$$T_{Hok}(t) = T_I(t) + T_{local}. \qquad (2)$$

Using this formula, we realize various transports of the SWC by adding the spatially and temporally constant eastward or westward wind stress over the Tsugaru Strait. This additional wind stress is expected to have little effect on the circulation in the Sea of Okhotsk except for the variation in the transport of the SWC, because the additional wind stress is free of curl and the Tsugaru Strait is far from the Sea of Okhotsk. The linear superposition, (2), is likely to be valid for the flow through the Soya Strait in the OGCM (see Fig. 3).

Varying the transport of the SWC in this way, we ran 17 experimental cases. The transport of the SWC averaged over the experiment period in each run is listed in Table 1. Time series of the transport of the SWC in five cases (A, C, I, L, N) are shown in Fig. 3. As the actual transport is estimated to be a maximum of about 1 Sv in summer (cf. Ebuchi *et al.*, 2006), Cases N and L appear to nearly represent the actual transport.

3. Overview of Circulation in the Sea of Okhotsk

In this section we briefly describe typical features of circulations reproduced in the model. In this and the next section we show the result of Case L since the transport of the SWC in this case approximates the actual one. In the central and northern part, a cyclonic gyre is formed, which is weak in summer and strong in winter. Figure 4 shows velocity field and salinity distribution at a depth of 20 m in summer (Fig. 4(a)) and in winter (Fig. 4(b)). It is shown that the ESC flowing southward along the east coast of Sakhalin is weak in summer and strong in winter in accordance with the seasonal variation of the wind-driven cyclonic gyre. The seasonal variability in the strength of the cyclonic gyre is consistent with previous studies, such as that of Ohshima *et al.* (2004). Another feature seen in Fig. 4 is an eastward flow around 47°N, which may be steered by bottom topography (Fig. 1). This eastward flow, together with the ESC, constitutes the southwestern part of the cyclonic gyre. On the other hand, a northward flow is seen in summer off the southern tip of Sakhalin (~144°E). This northward flow, with the eastward flow around 47°N, forms the anticyclonic gyre in the Kuril Basin. Some anticyclonic eddies are seen as well. These features, i.e. the anticyclonic gyre and the anticyclonic eddies in the Kuril Basin, were observed by satellite-tracked surface drifters (Ohshima *et al.*, 2002).

It is also shown that two different water masses intrude into the area off northeastern Hokkaido. Saline water of the SWC from the Japan Sea occupies the area in summer. On the other hand, fresher water carried by the ESC from the northwestern shelf is dominant in winter. The water mass change off the northeastern coast of Hokkaido represented in the model is consistent with the hydrographic analysis reported by Itoh and Ohshima (2000). This water mass change is related to the transport of the ESC and the SWC. Figure 5 shows the seasonal variations in the transport of the ESC and the SWC, which are calculated from the model results for two years from May 1999 to April 2001. Here, the transport of the ESC is defined as the transport by integrating the southward barotropic velocity at 53°N from the coast to the point where it vanishes. The transport of the SWC is defined as that flowing through the Soya Strait. The seasonal variations of the ESC and the SWC are simulated quite well (cf., for example, Matsuyama *et al.*, 1999; Itoh and

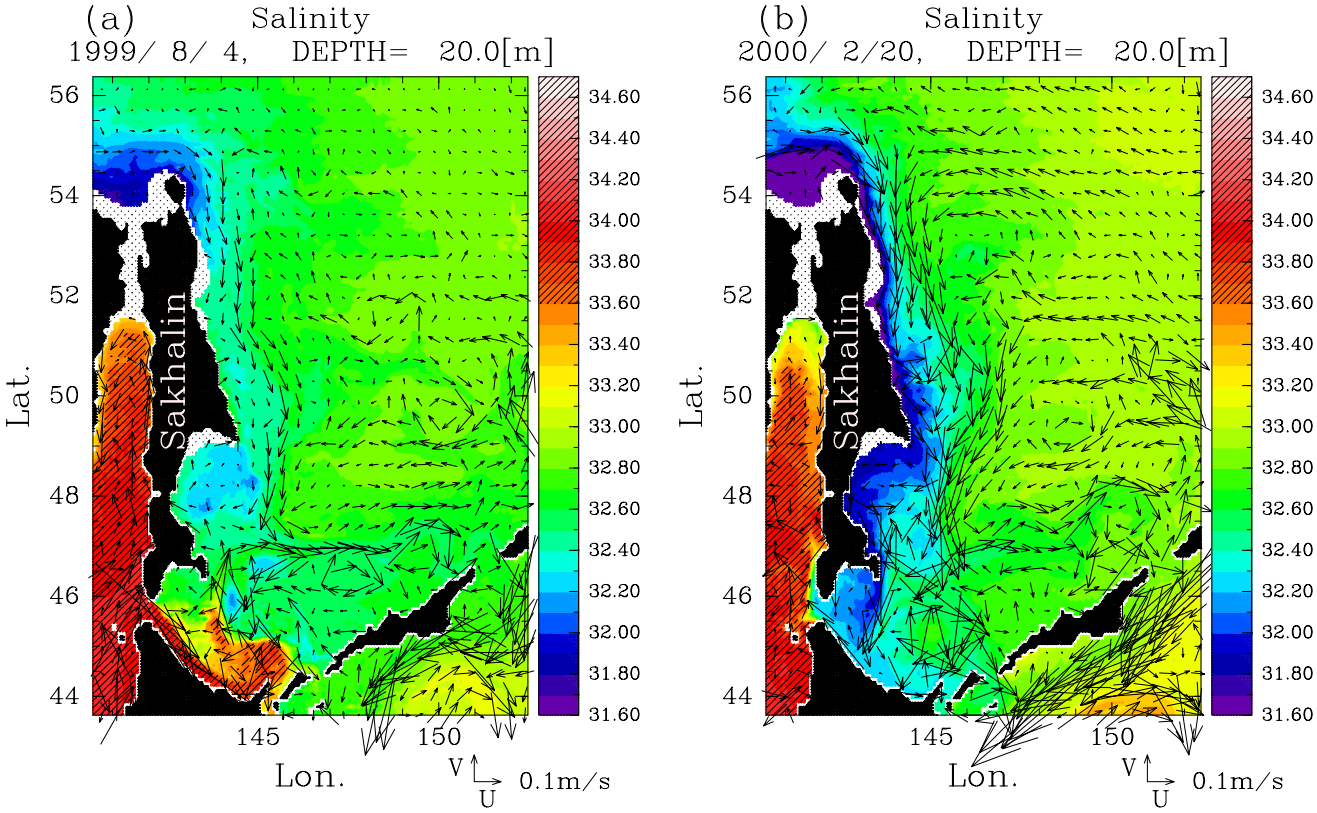

Fig. 4. Examples of salinity distribution and flow field at a depth of 20 m (a) in summer and (b) in winter in Case L. SWC Water is shaded.

Ohshima, 2000; Mizuta *et al*., 2003; Ebuchi, 2006; Ebuchi *et al*., 2006). The transport of the SWC is large in summer and small in winter. Although very few direct observations of the transport through the Soya Strait have been conducted, Ebuchi *et al*. (2006) have roughly estimated the transport from the surface velocity derived from the high frequency ocean radar. According to this estimation, it attains the maximum transport of around 1 Sv in summer. The transport of the SWC in the model is consistent with this. In contrast, the transport of the ESC is large in winter and small in summer. The transport of the ESC attains a maximum of about 10 Sv in February, which corresponds with the observation reported by Mizuta *et al*. (2003).

It should be noted that in Fig. 4(a) the nose of the SWC Water (shaded), which is defined as the water with salinity higher than 33.6 according to Itoh and Ohshima (2000), begins to swirl clockwise around the tip of the Shiretoko Peninsula around 145.5°E, 44.5°N. We focus on this eddy in the next section, and show that it is the WM eddy.

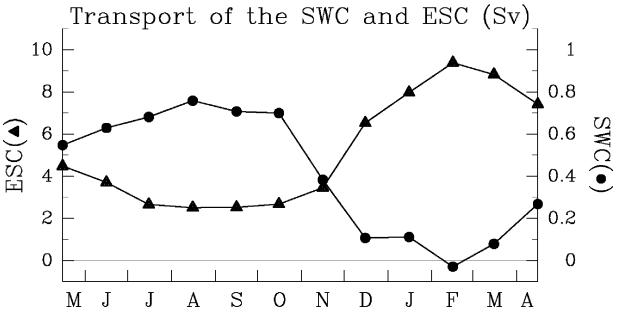

Fig. 5. Seasonal variations in the transport of the East Sakhalin Current at 53°N (triangles) and the Soya Warm Current (circles).

4. WM Eddy

Figures 6 and 7 show the flow field off Hokkaido at depths of 20 m and 60 m, respectively. The SWC Water is denoted by shading. When the SWC Water reaches off the tip of the Shiretoko Peninsula in July (Figs. 6(a) and 7(a)), it begins to swirl and evidence of an anticyclonic eddy appears around 145.5°E, 44.5°N. The SWC Water is not transported out through straits downstream but remains off the Shiretoko Peninsula, so that the eddy grows there subsequently (Figs. 6(b) and 7(b)). In September,

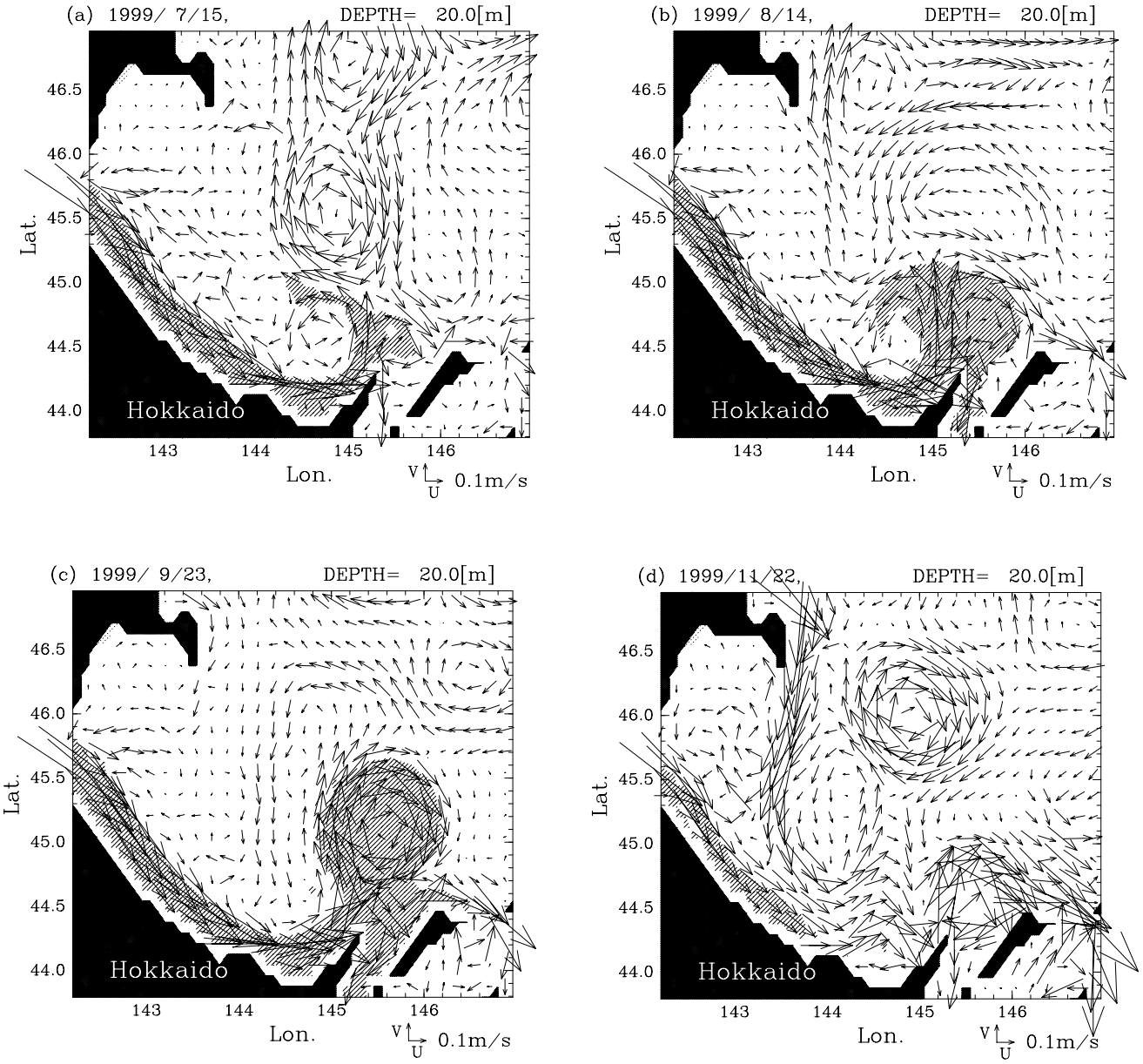

Fig. 6. Velocity field in Case L at a depth of 20 m off Hokkaido. The SWC Water is denoted by shading. (a) 15 July, (b) 14 August, (c) 23 September, and (d) 22 November. Note that the eddy around 144.8°E, 45.5°N in panel (a) is not the WM eddy.

the distinct eddy is finally formed accompanying a cyclonic eddy westward (Figs. 6(c) and 7(c)). After that, the eddy moves northward to become located around 145°E, 46°N (Figs. 6(d) and 7(d)). The location of the eddy in the model is consistent with that of the eddy observed by WM91 (compare Figs. 6(d) and 7(d) with figure 3 in WM91).

The flow fields at these two depths are almost identical, though the speed is a little larger at 20 m than at 60 m. The distribution of the SWC Water shows a few differences between these depths. Until September (panels (a)~(c) in both figures), the SWC Water around the eddy is distributed more widely at 20 m than at 60 m. In November (panel (d)), however, the SWC Water is not seen at 20 m within the eddy around 145°E, 46°N, but is still seen at 60 m. Moreover, the SWC Water along Hokkaido retreats from the Shiretoko Peninsula at 20 m, whereas it remains near the Shiretoko at 60 m.

Figure 8 displays the vertical section of the potential temperature, salinity, and potential density (σ_θ) across the eddy at 46°N on 22 November (see also Figs. 6(d) and 7(d)). A prominent feature is that the saline SWC

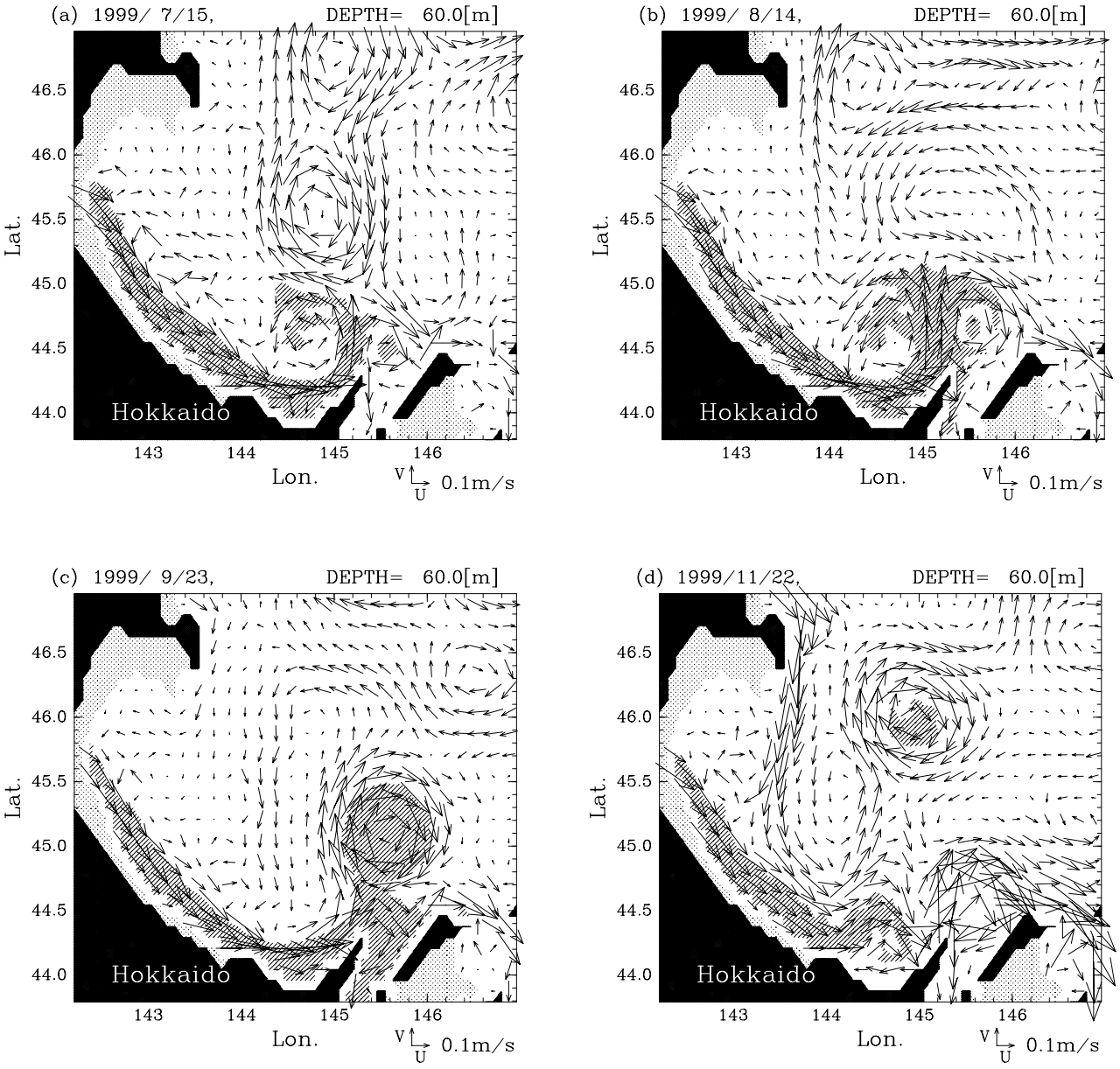

Fig. 7. As Fig. 6 but at a depth of 60 m. The region where the depth is shallower than 60 m is light-hatched.

Water rides over less saline water like a lens (Fig. 8(b)). This saline water is warm (Fig. 8(a)), so it is lighter than the surrounding water at the same depth (Fig. 8(c)). The coldest water exists around a depth of 400~600 m (Fig. 8(a)). The vertical structure of this eddy is qualitatively very similar to that observed by WM91 (see figure 4 in WM91), but there is a quantitative difference. The coldest water is less than 1°C in WM91, whereas it is about 2°C in the model. This is probably because the cold Dense Shelf Water (Shcherbina *et al*., 2004) is not formed over the northwestern shelf since our model does not include the ice formation processes.

Both the evolution of the eddy shown in Figs. 6 and 7, and the vertical structure shown in Fig. 8 illustrate that the formation of this eddy is caused by intrusion of the SWC Water into the Kuril Basin off the Shiretoko Peninsula, which is consistent with the discussion by WM91. Therefore, this eddy may be identified as the WM eddy.

5. Numerical Experiments

We have conducted numerical experiments to investigate dependency of the WM eddy formation on the trans-

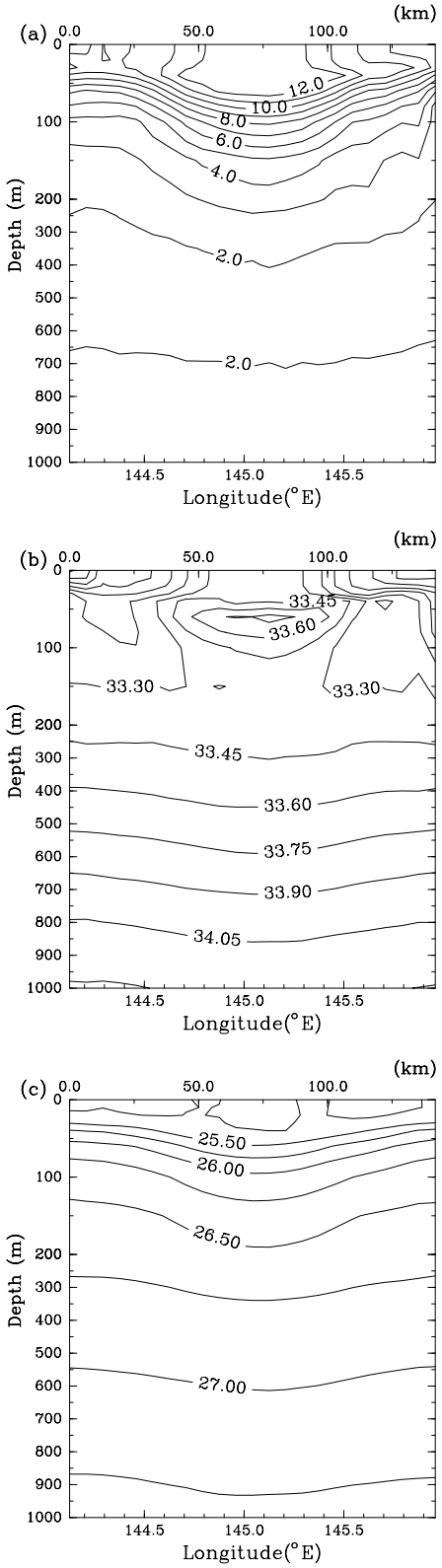

Fig. 8. Vertical sections of (a) potential temperature, (b) salinity, and (c) potential density (σ_θ) across the eddy at 46.0°N on 22 November in Case L. This figure is divided into two parts; the water structure above 200 m at an expanded scale and below it at a reduced scale.

port of the SWC. The transport of the SWC in each run is averaged over the experiment period, from 16 April to 23 September, as listed in Table. 1.

5.1 Results

Figure 9 shows the flow field and salinity higher than 33.6 psu, corresponding to the SWC Water, at a depth of 20 m on 23 September for four cases: Cases A, F, I and Q. Figure 9(a) shows those of Case A, where the mean transport of the SWC averaged over the experiment period is the smallest. In this case, the SWC Water is distributed only along the coast of Hokkaido west of the Shiretoko Peninsula. An indistinct eddy (which may be just a meander) forms at the tip of the peninsula; this eddy does not include SWC Water at any depth (not shown). As the transport increases, the eddy becomes distinct and enlarged, consisting of the SWC Water as in Cases F, I and Q (Figs. 9(b)–(d), see also Fig. 6(c) for Case L). In Case Q, the largest transport case (Fig. 9(d)), the SWC Water is far more widely distributed. The eddy does form but is skewed; a closed circulation is not well-defined on account of the large meander of the SWC.

The diameter and location of the eddy on 23 September, the last day of each experiment, are plotted in terms of the mean transport of the SWC during the experiment period in Fig. 10. Case Q is not included since the eddy is skewed as shown in Fig. 9(d). We define the northern and southern edges of the eddy (plus signs in Fig. 10) as the latitudes of the maximum eastward and westward velocity across the eddy at a depth of 20 m. The diameter (dots in Fig. 10) is defined as the distance between these edges. As the transport increases, its diameter gradually grows, reaching about 80 km. Regarding the eddy location, if the SWC transport is small (<0.55 Sv), the northern edge tends to move northward as the transport increases, whereas the southern edge remains at almost the same latitude, around 44.4°N.

In these cases, the eddy forms attached to Hokkaido or its neighboring island (Figs. 9(a) and (b)). The status of the eddy changes greatly at around 0.55 Sv. The southern edge of the eddy is separated from the coast (e.g. Fig. 9(c)) and tends to move northward (Fig. 6(d)) if the SWC transport exceeds 0.55 Sv. Since the transport of the actual SWC corresponds to that in Cases L~N, the model predicts that the WM eddy should form away from the coast, consistent with observations (WM91; Ebuchi, 2006).

Figure 10 indicates that the status of the eddy is categorized into two regimes; one regime has the WM eddy attached to the islands, while the other has the eddy separated from the islands.

To make the difference between the two regimes clearer, the calculations in Cases F and I are extended until November (Fig. 11, see also Fig. 6(d) for the Case

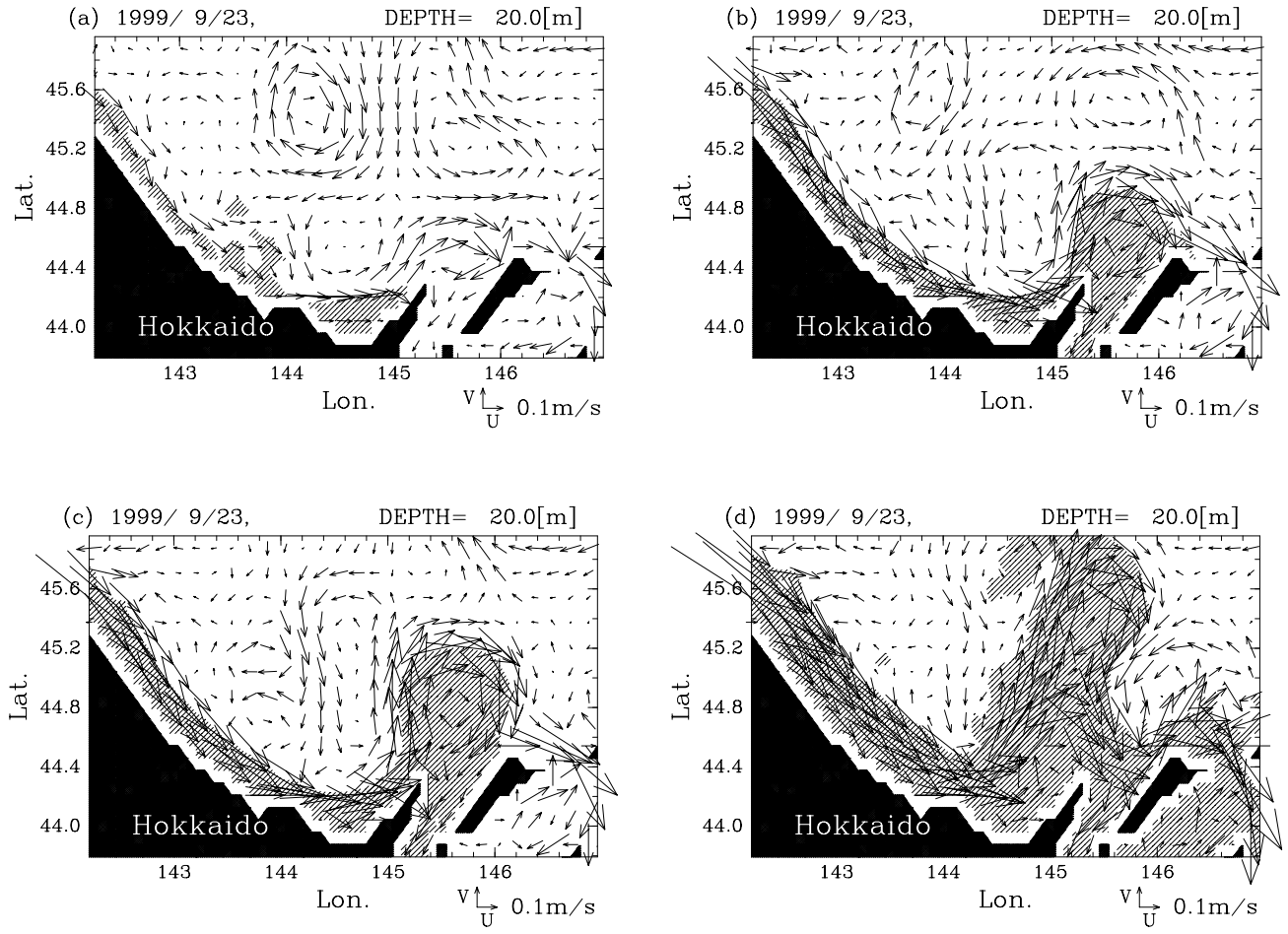

Fig. 9. Flow fields at a depth of 20 m around the eddy on 23 September of (a) Case A, (b) Case F, (c) Case I, and (d) Case Q. Waters with salinity higher than 33.6 (SWC Water) are the shaded regions.

L). In Case F, where the transport is less than 0.55 Sv, the eddy is proved to remain near the islands. On the other hand, in larger transport cases (e.g. Cases I and L), the eddy is separated from the islands as expected. There are two eddies in Case I (right panel of Fig. 11), i.e., one around 145.2°E, 45.3°N, and the other around 145.8°E, 46.5°N, because the WM eddy is divided into the two in Case I.

5.2 Discussion

Several theories have been proposed for the formation of an anticyclonic eddy generated by an outflow of a low-density, low potential vorticity water (for example, Kubokawa, 1991; Klinger, 1994; Nof and Pichevin, 1999). Kubokawa (1991) showed that an anticyclonic eddy forms if the outflow volume transport of the low potential vorticity fluid (regarded as low-density fluid) is larger than a critical value, which is the upper limit of the coastal flow downstream determined by a frontal wave theory. In our experiments the eddy becomes large as the trans-

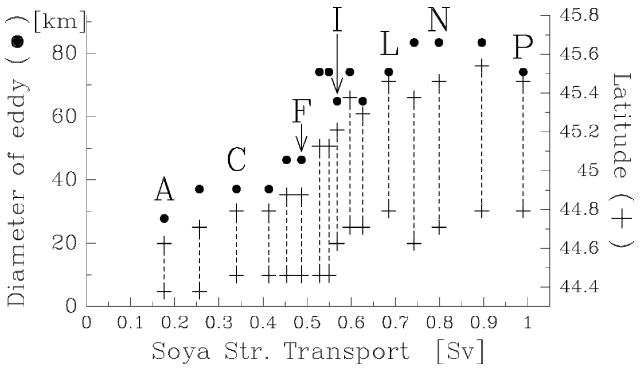

Fig. 10. Mean transport through the Soya Strait vs. diameter (dots), and the location of the WM eddy (dotted lines). Plus signs indicate the northern and southern edges of the eddy. The definition of the diameter and the edges are described in the text.

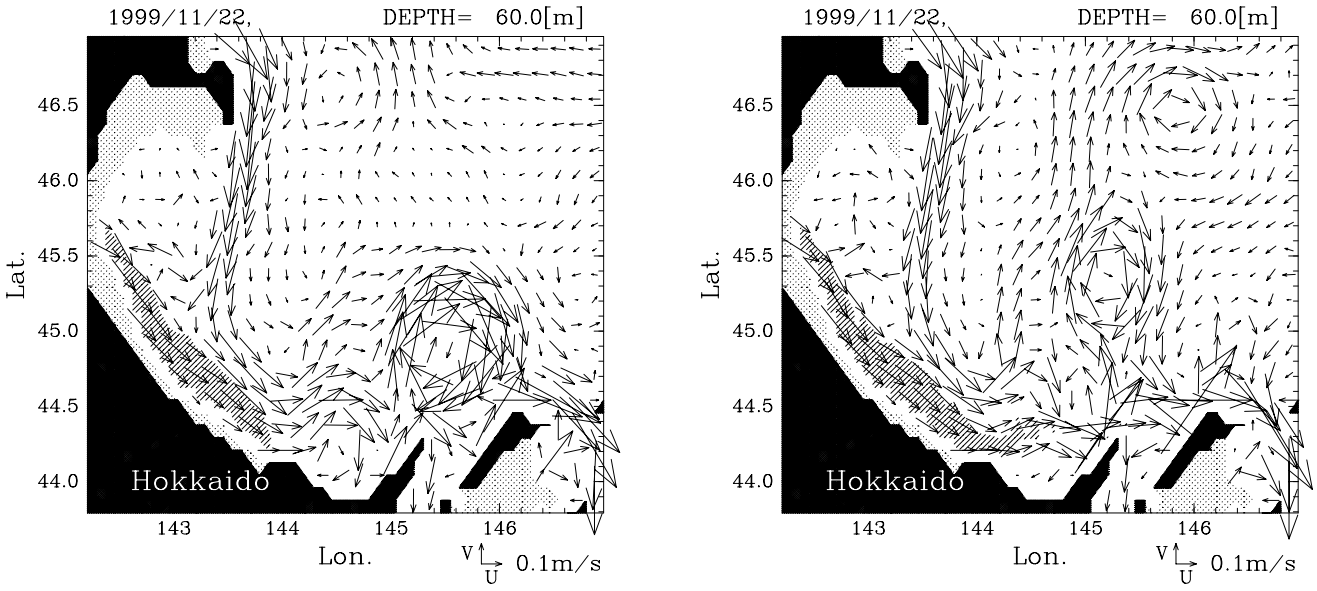

Fig. 11. Flow fields at a depth of 60 m around the eddy on 22 November of Case F (left) abd I (right). Waters with salinity higher than 33.6 (SWC Water) are the shaded regions.

port of the SWC increases. This reminds us of the theory of Kubokawa (1991), although, in our case, the downstream flow appears to be controlled by the flow through the Nemuro Strait and the Kunashiri Channel (refer to Fig. 1 for the geography). We consider that the eddy forms when the transport of the SWC exceeds that of the straits downstream. In order to examine this formation mechanism, we calculated transports through these straits. Figure 12 shows the time series of the SWC inflow from the Soya Strait (solid triangles) and the outflow from the straits downstream (solid circles). The panels (a) and (b) are for Cases A and L, whose flow fields are Fig. 9(a) (where the eddy does not form) and Figs. 6 and 7 (where the eddy forms distinctly), respectively.

We first look at Case A (Fig. 12(a)), in which the transport of the Soya Strait is the smallest. In this case, we expect that the transport of the SWC inflow is about equal to that of the outflow since a distinct eddy does not form. From May to June the SWC inflow balances the outflow from the straits, as expected. After July, however, there is an excess of outflow compared to the SWC inflow. This implies that there is an outflow of waters other than the SWC Water during summer. The excessive outflow from other sources, T_e, may be estimated as the difference between the total outflow transport and the SWC inflow of Case A if we assume that the transport of the SWC inflow is equal to that of the outflow when a distinct eddy does not form.

Now we look at Case L (Fig. 12(b)), where the eddy distinctly forms. The inflow transport of the SWC Water is large in May to July. However, we also see that there is excessive outflow in August and September. This suggests that this includes outflow from other sources, as in Case A. In order to retrieve the net outflow transport of the SWC Water in Case L, we subtract T_e from the total outflow transport, where we assume that the excessive transport from other sources is the same as that of Case A. As we expect, the net outflow (broken line) is smaller than the SWC inflow.

Figure 13 shows the relation between transport of the SWC inflow and that of the net outflow from the straits downstream, where each transport is averaged for the last half-period of the experiments (80 days). Note that the transport of the SWC differs from that in Table 1 because the averaging periods are different. When the transport of the inflow is small (Cases A~D), the transport of the outflow is balanced by that of inflow. On the other hand, the ratio of the outflow to the inflow transport reduces to 0.75 when the inflow transport is larger than about 0.7 Sv. The transition occurs roughly from Case F to Case I. In conjunction with Fig. 10, we can see that this transition transport corresponds with the transport for the regime transition in the eddy behavior. This is consistent with the mechanism published by Kubokawa (1991). Some readers may think that the geography in Kubokawa (1991) is too different from ours. However, we should recall that, in Kubokawa (1991), the transport is controlled by a frontal wave theory, where the mouth of the strait is essential. In the present study, on the other hand, the transport is controlled by flow through straits, so the difference in the geography is not important in this discussion.

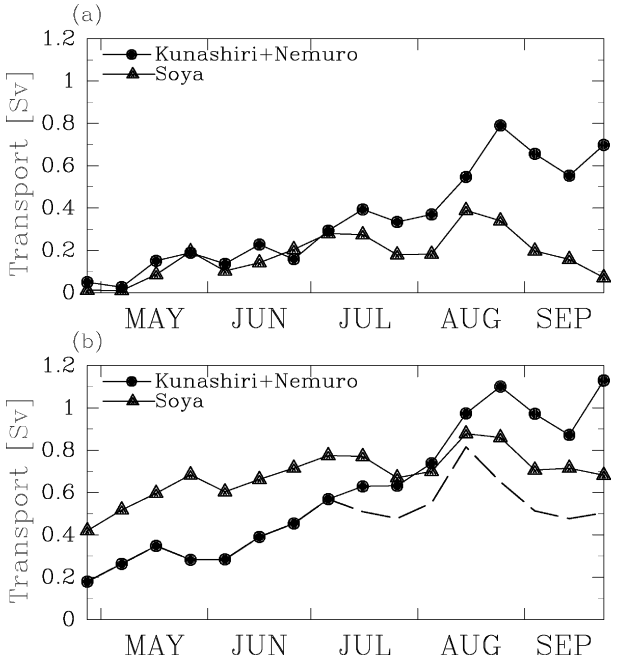

Fig. 12. Time series of transport of the inflow (solid triangles) and the outflow (solid circles). Inflow is defined as the flow through the Soya Strait, and outflow is defined as the flow through the Kunashiri Channel and the Nemuro Strait. *Net outflow* is plotted by a broken line. For the definition of *net outflow*, refer to text. (a) Case A and (b) Case L. Positive direction is defined as that flowing clockwise around Hokkaido.

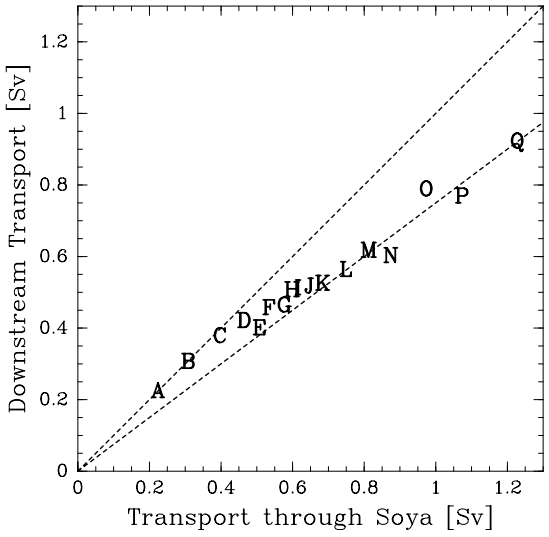

Fig. 13. Mean transport through the Soya Strait vs. transport through the straits downstream. Slopes of the two dotted straight lines are 1 and 0.75, respectively, representing the ratios of the outflow transport to the inflow transport.

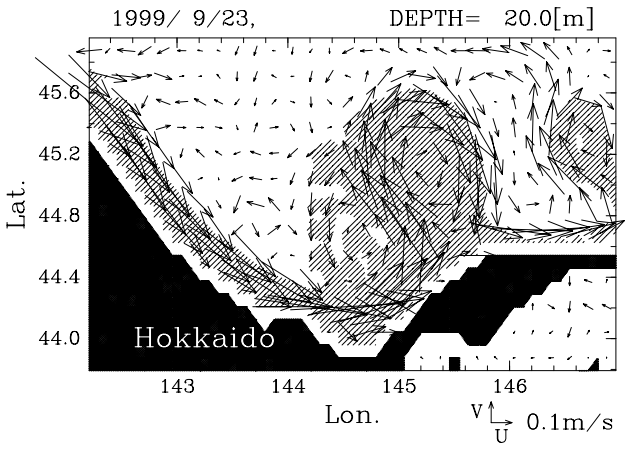

Fig. 14. Flow fields at a depth of 20 m around the eddy on 23 September in the case where the Nemuro Strait and the Kunashiri Channel are closed. Cf. Fig. 9(c), which is run with the same conditions except the geometry of the two straits. Waters with salinity higher than 33.6 (SWC Water) are the shaded regions.

As shown in Fig. 13, the increment in the transport of the outflow due to the additional wind stress over the Tsugaru Strait tends to be smaller than that of the SWC inflow. This may be curious from the viewpoint of the Island Rule because it suggests that the outflow transport should correspond to the inflow transport. The Island Rule is valid inasmuch as dissipation and the nonlinearity are ignored. The differential sensitivity to the additional wind stress between the transports in the Soya Strait and in the straits downstream (the Nemuro Strait and the Kunashiri Channel) implies that ignored terms in the Island Rule are not negligible in the straits. We do not elucidate this here, although we suspect that bottom and/or lateral friction causes reduction of the outflow transport from the straits adjacent to Hokkaido and redistributes it to remote straits along the Kuril Islands.

Nof and Pichevin (1999) showed that an anticyclonic eddy forms to balance the momentum associated with the southward downstream flow. In our numerical results, the downstream flow of the Soya Warm Current hugs the coast of Hokkaido almost southward (Fig. 6), which seems to be a similar situation to that described by Nof and Pichevin (1999).

An anticyclonic eddy can also form due to separation when the coastal current encounters a sharp convex corner (e.g. Klinger, 1994). The WM eddy in our model also forms when the SWC encounters a sharp corner, i.e. the tip of the Shiretoko Peninsula, consistent with the separation mechanism. In order to examine the effects of the sharp corner, we conducted an experiment with the same conditions as those of Case I, except that the both

the Nemuro Strait and the Kunashiri Channel are filled in (Fig. 14). In this case, the acute point associated with the Shiretoko Peninsula is changed to a straight coastline with an obtuse corner at the northern coast of the Kunashiri Island, as shown in the figure. Comparing Fig. 14 with Fig. 9(c) (Case I), we can see that the eddy forms at almost the same location, independent of the shape of the Nemuro/Kunashiri straits. Further, the eddy locates upstream from the obtuse corner of the Kunashiri. These results show that an acute angle corner is not necessary for the eddy to form, although the corner may be a trigger for the eddy formation, whether it is acute or obtuse.

Finally, we note that the depth along the Hokkaido begins to increase around the Shiretoko Peninsula (Fig. 1). There, the SWC Water ride over the denser water and the water column of the SWC Water is compressed. Hence, an anticyclonic eddy tends to form there. This water column compression is another candidate for the trigger, as well as the corner of the coastline is.

6. Summary

We have successfully reproduced various characteristics of the circulation of the Sea of Okhotsk by a high-resolution OGCM. In particular, the WM eddy (see Fig. 2) is satisfactorily reproduced in the model. The OGCM represents the seasonal variations in the transport of the Soya Warm Current (SWC) and the East Sakhalin Current (ESC) well, which leads to the water mass exchange in the southwestern part of the Sea of Okhotsk off the northeastern coast of Hokkaido. The area off Hokkaido is occupied by the saline Soya Warm Current Water (SWC Water) in summer, while fresher water of the ESC occupies it in winter. The WM eddy forms in late summer when the low-density SWC Water arrives off the Shiretoko Peninsula, as discussed in WM91. The structure and evolution of the eddy in WM91 are simulated well in the OGCM.

We carried out numerical experiments in which the transport of the SWC varied. It has been shown that the WM eddy formation depended upon the transport of the SWC. When the transport is small, a distinct eddy does not form. As the transport increases, its diameter becomes large up to about 80 km, and then the eddy moves northward accompanying a cyclonic eddy westward. It has been shown that the WM eddy is likely to be formed when the SWC inflow was larger than the net outflow from the straits downstream (cf. Kubokawa, 1991).

To improve the simulation of the Sea of Okhotsk, two processes should be considered. One is the sea ice. When the sea ice is produced, high density water is formed due to brine rejection. The cold Dense Shelf Water, the high density water produced in the northwestern shelf, is transported southward to the Kuril Basin by the ESC. This process is not included in our model, so the density stratification may not be represented well, especially in the southern part of the Sea of Okhotsk. In fact, the coldest water on the vertical section of the WM eddy in the model is not as cold as that in WM91, as discussed in Section 4. In addition, the existence of the sea ice affects the circulation by changing the surface stress. In a low resolution coupled ice-ocean model (1/2° in the zonal and 1/4° in the meridional direction), the extent of the sea ice cover in the Sea of Okhotsk has been simulated quite well (Ikeda *et al*., 2004; Watanabe *et al*., 2004). The simulation might be expected to improve if the ice model is coupled with the Okhotsk OGCM. The other process to be considered is the effects of tides. Tidal processes are thought to play important roles in modifying water properties (Nakamura *et al*., 2000; Nakamura and Awaji, 2004). Strong tidal currents even induce significant mean transport. In the North Pacific, it is one of the most important components in the formation of the North Pacific Intermediate Water. Tidal mixing is also important in generation of the eddies in the Kuril Basin (Ohshima *et al*., 2005). These issues remain for future work.

Acknowledgements

We acknowledge Director Prof. M. Wakatsuchi of the Institute of Low Temperature Science (ILTS), Hokkaido University, for his valuable comments. Thanks are extended to Dr. K. I. Ohshima and the membership of *Polar Seminar* in ILTS for helpful discussions. We are indebted to Dr. M. Itoh for providing the unpublished results. This paper improved greatly thanks to comments from an anonymous reviewer. The figures were produced by GFD-DENNOU Library (http://www.gfd-dennou.org/index.html.en). Numerical calculations were carried out on the SR8000 supercomputer at Hokkaido University Information Initiative Center and on the Origin350 at Hokkaido University Pan-Okhotsk Research Center. This study was partly supported by a Grant-in-Aid of the Ministry of Education, Culture, Sports, Science and Technology of Japan.

References

Boyer, T. P. and S. Levitus (1997): Objective Analysis of Temperature and Salinity for the World Ocean on a 1/4 Degree Grid. *World Ocean Atlas 1994, NOAA Atlas NESDIS*, **11**, 62 pp.

Ebuchi, N. (2006): Seasonal and interannual variations of the East Sakhalin Current observed by the TOPEX/POSEIDON altimeter. *J. Oceanogr*., **62**, 171–183.

Ebuchi, N., Y. Fukamachi, K. I. Ohshima, K. Shirasawa, M. Ishikawa, T. Takatsuka, T. Daibo and M. Wakatsuchi (2006): Observation of the Soya Warm Current using HF ocean radar. *J. Oceanogr*., **62**, 47–61.

Godfrey, J. S. (1989): A Sverdrup model of the depth-integrated flow from the world ocean allowing for island circulations. *Geophys. Astrophys. Fluid Dyn*., **45**, 89–112.

Ikeda, M., H. Shinkai and T. Watanabe (2004): Parametrization of thin ice in a coupled ice-ocean model: Application to the seasonal ice cover in the sea of Okhotsk. *Atmosphere-Ocean*, **42**, 1–12.

Itoh, M. and K. I. Ohshima (2000): Seasonal variations of water masses and sea level in the southwestern part of the Okhotsk Sea. *J. Oceanogr.*, **56**, 643–654.

Klinger, B. A. (1994): Baroclinic eddy generation at a sharp corner in a rotating system. *J. Geophys. Res.*, **99**, 12515–12531.

Kubokawa, A. (1991): On the behavior of outflows with low potential vorticity from a sea strait. *Tellus*, **43A**, 168–176.

Levitus, S., R. Burgett and T. P. Boyer (1994): Salinity. *World Ocean Atlas 1994*. *NOAA Atlas NESDIS*, **3**, 99 pp.

Liu, W. T., W. Tang and P. S. Polito (1998): NASA scatterometer global ocean-surface wind fields with more structures than numerical weather prediction. *Geophys. Res. Lett.*, **25**, 761–764.

Liu, Z., L. Wu and H. Hurlburt (1999): Rossby wave-coastal Kelvin wave interaction in the extratropics. part II: Formation of island circulation. *J. Phys. Oceanogr.*, **29**, 2405–2418.

Matsuyama, M., M. Aota, I. Ogasawara and S. Matsuyama (1999): Seasonal variation of Soya Current. *Umi no Kenkyu*, **8**, 333–338 (in Japanese with English abstract).

Mellor, G. L. and T. Yamada (1982): Development of a turbulence closure model for geophysical fluid problems. *Rev. Geophys. Space Phys.*, **20**, 851–875.

Mellor, G. L., T. Ezer and L.-Y. Oey (1994): The pressure gradient conundrum of sigma coordinate ocean models. *J. Atmos. Oceanic Technol.*, **11**, 1126–1134.

Mellor, G. L., S. Häkkinen, T. Ezer and R. Patchen (2002): A generalization of a sigma coordinate ocean model and an intercomparison of model vertical grids. p. 55–72. In *Ocean Forecasting: Conceptual Basis and Applications*, ed. by N. Pinardi and J. D. Woods, Springer, Berlin.

Mizuta, G., Y. Fukamachi, K. I. Ohshima and M. Wakatsuchi (2003): Structure and seasonal variability of the East Sakhalin Current. *J. Phys. Oceanogr.*, **33**, 2430–2445.

Nakamura, T. and T. Awaji (2004): Tidally induced diapycnal mixing in the Kuril Straits and its role in water transformation and transport: A three-dimensional nonhydrostatic model experiment. *J. Geophys. Res.*, **109**, C09S07, doi:10.1029/2003JC001850.

Nakamura, T., T. Awaji, T. Hatayama, K. Akitomo, T. Takizawa, T. Kono, Y. Kawasaki and M. Fukasawa (2000): The generation of large-amplitude unsteady lee waves by subinertial K_1 tidal flow: A possible vertical mixing mechanism in the Kuril Straits. *J. Phys. Oceanogr.*, **30**, 1601–1621.

Nof, D. and T. Pichevin (1999): The establishment of the Tsugaru and the Alboran gyres. *J. Phys. Oceanogr.*, **29**, 39–54.

Ohshima, K. I., M. Wakatsuchi, Y. Fukamachi and G. Mizuta (2002): Near-surface circulation and tidal currents of the Okhotsk Sea observed with satellite-tracked drifters. *J. Geophys. Res.*, **107**, 3195, doi:10.1029/2001JC001005.

Ohshima, K. I., D. Simizu, M. Itoh, G. Mizuta, Y. Fukamachi, S. C. Riser and M. Wakatsuchi (2004): Sverdrup balance and the cyclonic gyre in the Sea of Okhotsk. *J. Phys. Oceanogr.*, **34**, 513–525.

Ohshima, K. I., Y. Fukamachi, T. Mutoh and M. Wakatsuchi (2005): A generation mechanism for mesoscale eddies in the Kuril Basin of the Okhotsk Sea: Baroclinic instability caused by enhanced tidal mixing. *J. Oceanogr.*, **61**, 247–260.

Shcherbina, A. Y., L. D. Talley and D. L. Rudnick (2004): Dense water formation on the northwestern shelf of the Okhotsk Sea: 1. Direct observation of brine rejection. *J. Geophys. Res.*, **109**, doi:10.1029/2003JC002196.

Simizu, D. and K. I. Ohshima (2002): Barotropic response of the sea of Okhotsk to wind forcing. *J. Oceanogr.*, **58**, 851–860.

Simizu, D. and K. I. Ohshima (2006): A model simulation on the circulation in the Sea of Okhotsk and the East Sakhalin Current. *J. Geophys. Res.*, **111**, C05016, doi:10.1029/2005JC002980.

Smagorinsky, J. (1963): General circulation experiments with the primitive equations. I. The basic experiment. *Mon. Weather Rev.*, **91**, 99–164.

Wakatsuchi, M. and S. Martin (1991): Water circulation in the Kuril Basin of the Okhotsk Sea and its relation to eddy formation. *J. Oceanogr. Soc. Japan*, **47**, 152–168.

Watanabe, T., M. Ikeda and M. Wakatsuchi (2004): Thermohaline effects of the seasonal sea ice cover in the Sea of Okhotsk. *J. Geophys. Res.*, **109**, C09S02, doi:10.1029/2003JC001905.